Computational Study of Negative Differential Resistance in Graphene Bilayer Nanostructures

K. M. Masum Habib, Sonia Ahsan and Roger K. Lake

Department of Electrical Engineering, University of California, Riverside, CA 92521-0204

ABSTRACT

Although graphene has fascinating electronic properties, lack of a band-gap reduces its utility for conventional electronic device applications. A tunable bandgap can be induced in bilayer graphene by application of a potential difference between the two layers. The simplest geometry for creating such a potential difference consists of two overlapping single layer graphene nanoribbons. Numerical simulations, based on π-band nearest neighbor tight binding model and the non-equilibrium Green's function formalism, show that transmission through such a structure has a strong dependence on applied bias. The simulated current voltage characteristics mimic the characteristics of resonant tunneling diode featuring negative differential resistance. It is found that the bandgap of the nanoribbons and length of the bilayer region have significant effects on the current voltage characteristics. In particular, the peak to valley ratio decreases with increasing length of the bilayer region. And the cut-in voltage is strongly modulated by the bandgap of the GNRs.

Keywords: Graphene, Bilayer, Negative Differential Resistance, NEGF.

1. INTRODUCTION

In graphene, a sheet of carbon atoms arranged in a honeycomb structure, electrons can move as massless Dirac fermions [1] with extremely high mobility ($\sim 10^5$ cm^{2}V^{-1}s^{-1})[2] and a long coherence length ($\sim \mu$m). Although it has fascinating electronic properties, lack of a bandgap[3] in two-dimensional (2D) graphene reduces its utility for conventional electronic device applications. Compared to 2D graphene sheet, quasi one dimensional, narrow ($<$10nm) ribbons, better known as graphene nanoribbons (GNRs)[4,5] show distinct electronic properties with semiconducting band structures with controllable bandgaps. A tunable bandgap can also be induced by stacking two monolayers of graphene to form a bilayer, which has a zero bandgap semiconducting band structure,[6] and creating potential difference in between.[7,8]

The possibility of Field Effect Transistors (FETs) using bilayer graphene as the channel material was recently studied.[9] It was shown that this FET has poor I_{on}/I_{off} due to strong band-to-band tunneling. However, a tunnel FET (TFET) using bilayer graphene showed promising performance.[10] Other proposed devices include a nanoelectromechanical FET based on interlayer distance modulation,[11,12] a FET utilizing a bilayer exciton condensate,[13] $p-n$ junctions,[14] $p-n-p$ junctions[15,16] etc.

Negative differential resistance (NDR) was predicted to occur in devices based on single-gated graphene sheet,[17] chemical doping in GNR[18] and strained GNR.[19] Do *et al.* demonstrated that NDR can be observed in p^+-p junctions of zigzag GNRs created by field-effect doping.[20] Recently, a strong NDR behavior was also predicted in $p-n$ junction of single layer chemically or electrically doped graphene.[21] However, many of these FET and NDR type devices have multiple gates making them relatively complex structures.

The electronic transport properties of a simple bilayer GNR geometry, consists of two single layer GNRs placed on top of each other either in AA or in AB stacking, was recently studied.[22] In this arrangement, a bias is applied to the top GNR with respect to the bottom one by independently contacting each GNR. It was shown that proposed geometry with this biasing scheme results in NDR. In this work, we study the effects of (i) the length of the bilayer region, and (ii) bandgap of the GNRs on the current voltage characteristics of the geometry using π-bond nearest neighbor tight binding model and non-equilibrium Green's function formalism (NEGF). It is found that the bandgap of the nanoribbons and length of the bilayer region have significant effects on the current voltage characteristics. In particular the peak to valley ratio decreases with increasing length of the bilayer region. And the cut-in voltage depends on the bandgap of the GNRs.

Send correspondence to K. M. M. Habib, E-mail: khabib@ee.ucr.edu

Carbon Nanotubes, Graphene, and Associated Devices IV, edited by Didier Pribat, Young-Hee Lee, Manijeh Razeghi,
Proc. of SPIE Vol. 8101, 81010Q · © 2011 SPIE · CCC code: 0277-786X/11/$18 · doi: 10.1117/12.894252

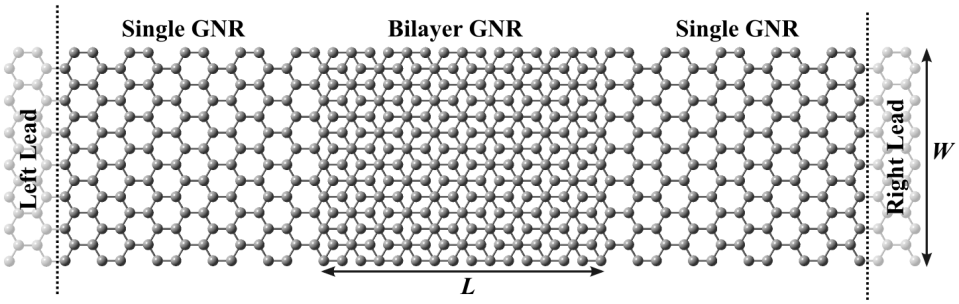

Figure 1. Atomistic geometry of 14-AGNR AB bilayer structure. The length of the bilayer region is 2.13 nm. The width of the GNR is 1.6 nm. The left and the right leads are semi-infinite GNRs modeled using self-energies.

2. METHOD

A model bilayer GNR structure is shown in Fig. 1. This bilayer geometry consists of two single layer armchair type GNRs (AGNRs) placed one top of each other forming an AB stacked central bilayer region. A bias is applied to the right lead with respect to the left one. In order to study the effects of the length, L, of the bilayer region, we have considered three structures with $L = 1.28, 1.70$ and 2.13 nm. The widths, W, of the GNRs of these structures are chosen to be 14 ($3n + 2$) C atomic layers, approximately 1.60 nm to minimize the effects of bandgap resulting from finite width. The bandgap of the single layer 14-AGNR, calculated from π bond tight binding model is zero. In order to study the effects of bandgap on $I - V$ characteristics, we have also considered geometries consisting of 15 and 16 -C atomic layers, ~ 1.72 and ~ 1.84 nm wide AGNRs, respectively, while keeping the bilayer length fixed at 1.70 nm.

We model the electronic properties of the GNRs using π-band nearest neighbor tight binding Hamiltonian as the low energy properties of graphene are mainly determined by the p_z orbitals. The tight binding Hamiltonian for the geometry shown in Fig. 1 is given by,[23]

$$H = -t_0 \sum_{\langle i,j\rangle,m} (a^+_{m,i} b_{m,j} + H.C.) - t_1 \sum_i (a^+_{1,i} b_{2,i} + H.C.) \tag{1}$$

where, $a_{m,i}(b_{m,i})$ annihilates an electron on sublattice A(B), in GNR $m = 1, 2$, at lattice site i. The subscript $\langle i, j\rangle$ represents a pair of nearest neighbors in the same GNR. In AB stacking, the atoms on the A sublattice of the bottom GNR (A_1) are connected to the B sublattice of the top GNR (B_2). The in plane interaction between the nearest neighbors is given by the hopping parameter, $t_0 = 2.66$ and the interlayer coupling is modeled by the hopping parameter, $t_1 = 0.1t_0$.[23]

The transport calculations start with the generation of real-space Hamiltonian matrix elements for the geometry shown in Fig. 1. The matrix elements of external potential energy, U are calculated as $\langle i|U|j\rangle = \delta_{i,j} [U(\mathbf{r}_i) + U(\mathbf{r}_j)]/2$ where, the indices i and j label the atoms, and $\delta_{i,j}$ is the Kronecker delta function. The applied bias is modeled by shifting the potential energies of the right and the left GNRs by $-eV/2$ and $eV/2$ amounts, respectively, where, V is the bias voltage, i. e., $U(\mathbf{r}_i) = -eV/2$ for atoms on right GNR and, $U(\mathbf{r}_i) = eV/2$ for atoms on the left GNR. This approach in which the matrix elements have the same form as in an extended Huckel model has been used by others. [24] The approach captures the Stark effect, but not non-equilibrium self-consistency.

These and the π-band Hamiltonian matrix elements are used in the recursive Green's function (RGF) algorithm to calculate the surface self-energies of left and right contacts, $\mathbf{\Sigma}^l$ and $\mathbf{\Sigma}^r$ respectively and, the Green's function of the device, $\mathbf{G}^R$, as described in Ref.[25] The transmission spectrum, $T(E)$, is then calculated from the standard Green's function expression,

$$T(E) \;=\; \mathrm{tr}\left\{\mathbf{\Gamma}^l_{1,1}\mathbf{G}^R_{1,N}\mathbf{\Gamma}^r_{N,N}(\mathbf{G}^R_{1,N})^\dagger\right\} \tag{2}$$

where, the indices 1 and N in Eq. (2) indicate the first and last block-layers of the left GNR and right GNR respectively, $\mathbf{\Gamma}^l_{1,1} \;=\; i\left(\mathbf{\Sigma}^l - \mathbf{\Sigma}^{l\dagger}\right)$,and $\mathbf{\Gamma}^r_{N,N} \;=\; i\left(\mathbf{\Sigma}^r - \mathbf{\Sigma}^{r\dagger}\right)$. The coherent current is calculated using the Landauer-Buttiker formalism,

$$I = \frac{2e}{\hbar}\int \frac{dE}{2\pi} T(E)\left[f(E - (\mu_l + eV/2)) \;-\; f(E - (\mu_r - eV/2))\right] \tag{3}$$

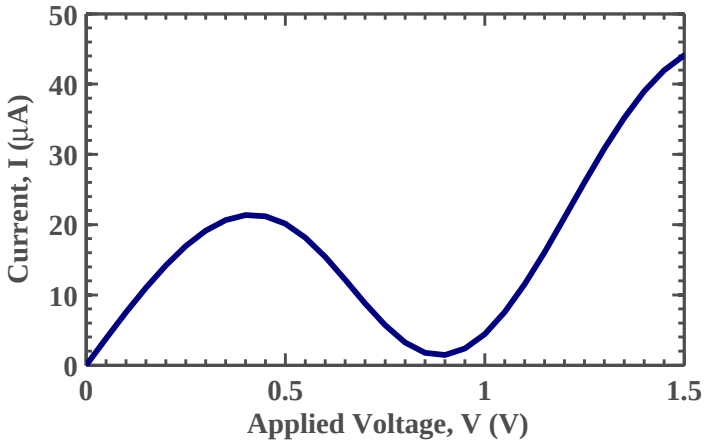

Figure 2. (Color Online) Simulated Current Voltage ($I-V$) characteristics of 14-AGNR bilayer with $L = 2.13$ nm exhibiting NDR. The peak and valley currents are $\sim 21.36\mu$A and $\sim 1.54\mu$A, occur at 0.4 V and 0.9 V respectively.

where, $f(E)$ is the Fermi function, and μ_l and μ_r are the fermi levels of the left and right contacts, respectively. In all our calculations we have assumed room temperature, $T = 300$ K.

3. RESULTS AND DISCUSSION

The simulated $I-V$ characteristics of 14-AGNR bilayer structure corresponding to Fig. 1 are shown in Fig. 2 exhibiting NDR. The peak and valley currents are $\sim 21.36\mu$A and $\sim 1.54\mu$A, occur at 0.4 V and 0.9 V respectively. These results are consistent with the results from *ab initio* calculations.[22]

In order to understand the origin of NDR in the $I-V$ characteristics we plot the transmission coefficient as a function of energy for different bias voltages as shown in Fig. 3. In agreement with and as discussed by, [23] the unbiased transmission shows a Fabry-Perot resonant feature at low energy and both resonances and antiresonances at more excited energies. The transmission coefficient for unbiased bilayer near $E = 0$ is almost 1. This can be well understood by noticing that the band structure of bi- and single-layer 14-AGNR calculated from π band model do not have a bandgap. The dips near ± 0.5 V are the anti-resonant points which occur due to destructive interference between the reflected electronic waves coming from the potential discontinuities at the cut ends of the left and the right GNR.

The application of a bias shifts the band structures of the left and right GNRs up and down, respectively, leading to wavevector mismatch between the GNRs[20,22,26] which, in turn, results in low transmission coefficient as shown in Fig. 3. With the bias increased further, the band structures are moved further and wavevector mismatch becomes more pronounced which results in even stronger suppression of transmission over a large energy window. Near $V = 0.8$ V, the transmission is very strongly suppressed. An increment of bias beyond this point, however, caused the transmission to increase again since other excited subbands come into play.

The coherent current at any bias is proportional to the area under the transmission curve bounded by the Fermi levels of the contacts. As the bias is increased from 0 V, the quasi-fermi levels of the contacts go away from each other opening an energy window of integration. As the bias increases, this energy window also increases but the transmission decreases. Initially the increasing energy window becomes dominant over the decreasing transmission leading to increasing area under the transmission curve which, in turn, results in increasing current. With the bias increased, however, decreasing transmission coefficient dominates over the increasing energy window leading to smaller area which, in turn, results in low current. Having understood the $I-V$ characteristics of 14-AGNR bilayer, we are now ready for the effects of bilayer length and bandgap of GNRs.

The $I-V$ characteristics of the proposed bilayer structure show a significant dependence on the length, L, of the bilayer region as indicated in Fig. 4. In particular, the peak current decreases while the valley current increases with L thus peak to valley ration decreases. The results are summarized in Table 1.

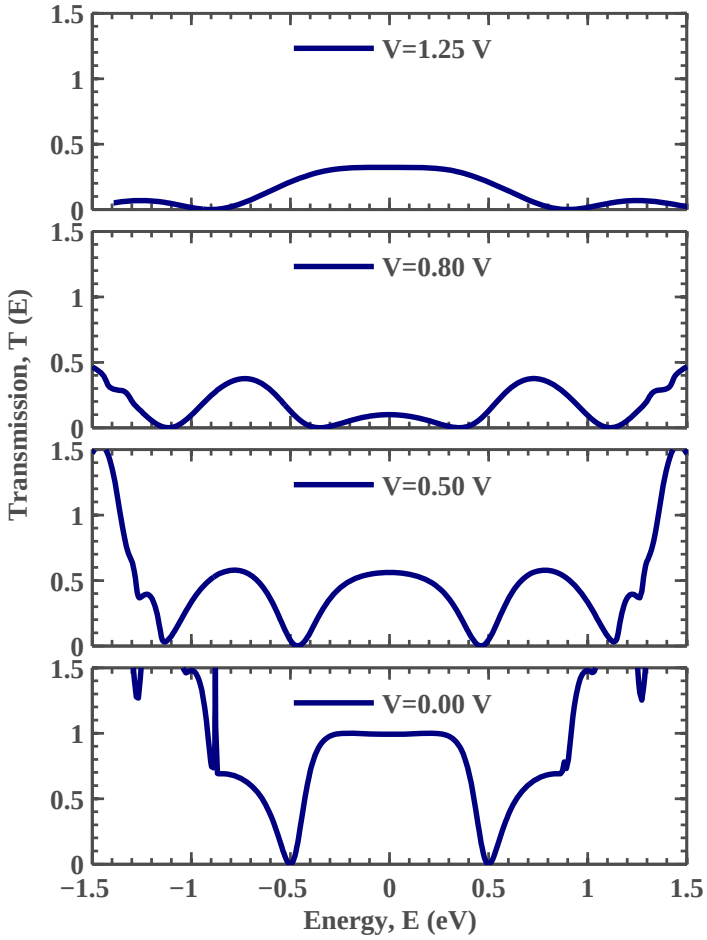

Figure 3. (Color Online) Transmission coefficient as a function of energy for different bias voltages ($L = 2.13$ nm and $W = 1.60$ nm). The application of a bias shifts the band structures of the left and right GNRs up and down, respectively, leading to wavevector mismatch between the GNRs which, in turn, results in low transmission coefficient.

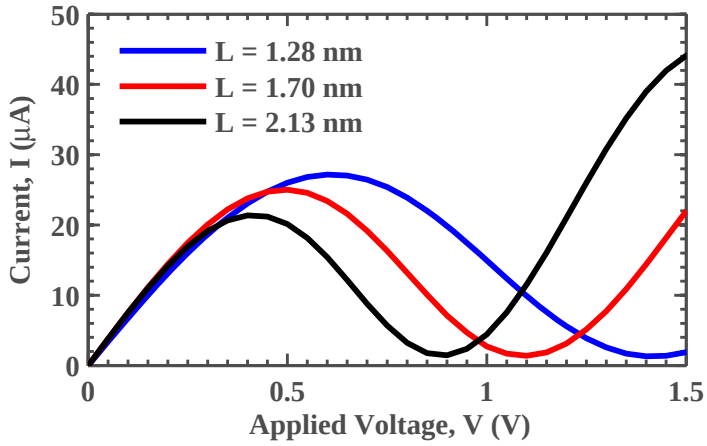

Figure 4. (Color Online) Simulated Current–Voltage ($I - V$) characteristics of 14-AGNR bilayer for different lengths of the bilayer region. The peak to valley ratio decreases with increasing bilayer length.

L (nm)	V_{peak} (V)	V_{valley} (V)	I_{peak} (μA)	I_{valley} (μA)	I_{peak}/I_{valley}
1.28	0.65	1.45	27.04	1.37	19.7
1.70	0.50	1.10	25.02	1.38	18.13
2.13	0.40	0.90	21.36	1.54	13.87

Table 1. Calculated peak and valley currents for different lengths of the bilayer region of 14-AGNR structures.

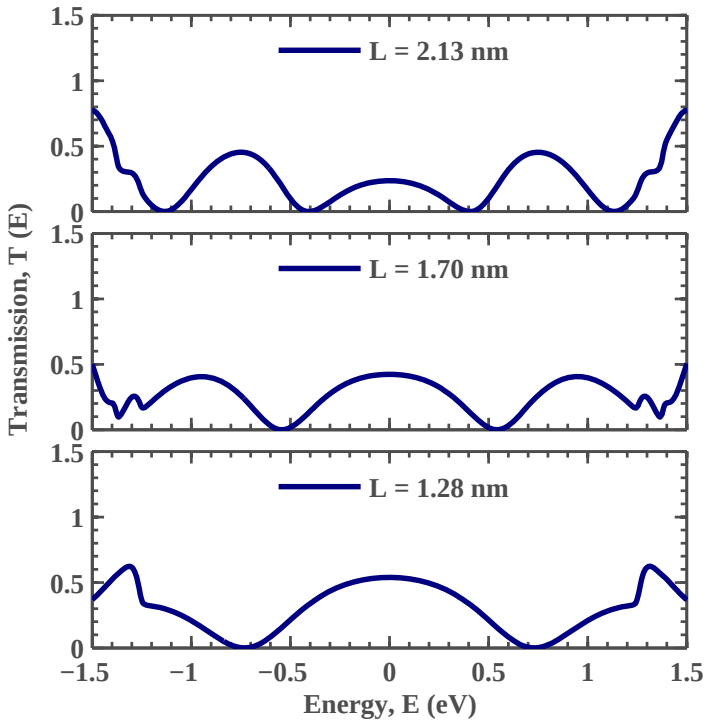

Figure 5. (Color Online) Transmission coefficient as a function of energy at $V = 0.7$ V for different bilayer lengths ($W = 1.60$ nm). The transmission for $L = 2.13$ nm is suppressed most. The transmission is suppressed least for $L = 1.28$ nm.

The effects of length on $I - V$ can be explained with the help of transmission plots for different bilayer lengths at $V = 0.7$ V as shown in Fig. 5. At the same bias voltage, the transmission for $L = 2.13$ nm is suppressed most. The transmission is suppressed least for $L = 1.28$ nm. This leads to minimum peak to valley ratio for $L = 2.13$ nm structure while maximum peak to valley ratio for $L = 1.28$ nm.

In all the results discussed above we have used 14-AGNR which has a band structure similar to 2D graphene sheet with zero bandgap linear dispersion relationship. In order to see the effects of bandgap on $I - V$ characteristics, we have simulated structures consisting of 15 and 16-C atomic layer wide GNRs that are ~ 1.72 and ~ 1.84 nm respectively. The 15- and 16-AGNR have bandgaps of ~ 0.59 eV and ~ 0.58 eV respectively. The calculated current voltage characteristics are shown in Fig. 6. In the bilayer structure consisting of 15-AGNRs, for bias voltages upto ~ 0.6 V the current is very small due to the bandgap. For 16-AGNR case, however, the current is suppressed upto ~ 0.9 V which cannot be explained by the bandgap anymore.

The transmission plots shown in Fig. 7 for structures with different widths are also consistent with the current voltage characteristics. For 15-AGNR (see $W = 1.72$ nm), the transmission is suppressed over an energy window of ~ 0.6 eV due to bandgap of the GNRs. For 16-AGNR case, the transmission is strongly suppressed over ~ 1.1 eV; the origin of which is not well understood at this point and will be addressed elsewhere.

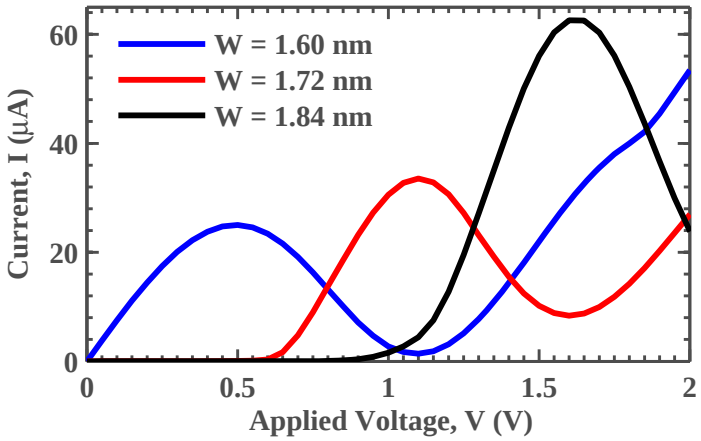

Figure 6. (Color Online) Simulated Current–Voltage ($I - V$) characteristics of bilayer structures with different widths ($L = 1.70$ nm). The cut-in voltage strongly depends on the GNR bandgap which, in turn, depends on GNR width.

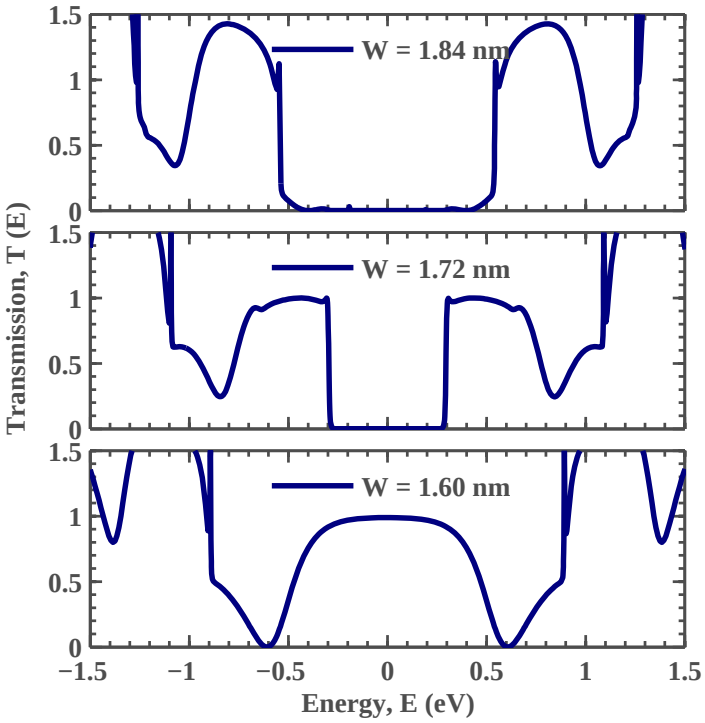

Figure 7. (Color Online) Transmission coefficient for different GNR widths as a function of energy ($L = 1.70$ nm). For 15-AGNR ($W = 1.72$ nm), the transmission is suppressed over an energy window of ~ 0.6 eV due to bandgap of the GNRs. For 16-AGNR case, the transmission is strongly suppressed over ~ 1.1 eV.

4. CONCLUSION

In this work we study the effects of length of bilayer region and the bandgap of the GNRs on the electronic transport properties of a simple bilayer GNR structure consisting of two single layer GNRs placed on top of each other in AB stacking sequence. Calculations, based on π-band nearest neighbor tight binding model and non-equilibrium Green's function formalism, show that NDR occurs in such structures. It is found that the bandgap of the nanoribbons and length of the bilayer region have significant effects on the current voltage characteristics. In particular the peak to valley ratio decreases with increasing length of the bilayer region. And the cut-in voltage depends on the bandgap of the GNRs.

ACKNOWLEDGMENTS

This work is supported by the Microelectronics Advanced Research Corporation Focus Center on Nano Materials (FENA).

REFERENCES

[1] Novoselov, K. S., Geim, A. K., Morozov, S. V., Jiang, D., Katsnelson, M. I., Grigorieva, I. V., Dubonos, S. V., and Firsov, A. A., "Two-dimensional gas of massless dirac fermions in graphene," *Nature* **438**, 197–200 (November 2005).

[2] Novoselov, K. S., Geim, A. K., Morozov, S. V., Jiang, D., Zhang, Y., Dubonos, S. V., Grigorieva, I. V., and Firsov, A. A., "Electric Field Effect in Atomically Thin Carbon Films," *Science* **306**(5696), 666–669 (2004).

[3] Ando, T., "Exotic electronic and transport properties of graphene," *Physica E: Low-dimensional Systems and Nanostructures* **40**(2), 213 – 227 (2007).

[4] Li, X., Wang, X., Zhang, L., Lee, S., and Dai, H., "Chemically Derived, Ultrasmooth Graphene Nanoribbon Semiconductors," *Science* **319**(5867), 1229–1232 (2008).

[5] Lam, K.-T. and Liang, G., "An ab initio study on energy gap of bilayer graphene nanoribbons with armchair edges," *Applied Physics Letters* **92**(22), 223106 (2008).

[6] Lu, C. L., Chang, C. P., Huang, Y. C., Lu, J. M., Hwang, C. C., and Lin, M. F., "Low-energy electronic properties of the ab-stacked few-layer graphites," *Journal of Physics: Condensed Matter* **18**(26), 5849 (2006).

[7] Min, H., Sahu, B., Banerjee, S. K., and MacDonald, A. H., "Ab initio theory of gate induced gaps in graphene bilayers," *Phys. Rev. B* **75**, 155115 (Apr 2007).

[8] Zhang, Y., Tang, T.-T., Girit, C., Hao, Z., Martin, M. C., Zettl, A., Crommie, M. F., Shen, Y. R., and Wang, F., "Direct observation of a widely tunable bandgap in bilayer graphene," *Nature* **459**(7248), 820 (2009).

[9] Fiori, G. and Iannaccone, G., "On the Possibility of Tunable-Gap Bilayer Graphene FET," *IEEE Electron Device Letters* **30**, 261–264 (March 2009).

[10] Fiori, G. and Iannaccone, G., "Ultralow-Voltage Bilayer Graphene Tunnel FET," *IEEE Electron Device Letters* **30**, 1096–1098 (Oct 2009).

[11] Lam, K.-T. and Liang, G., "A computational evaluation of the designs of a novel nanoelectromechanical switch based on bilayer graphene nanoribbon," in [*IEEE Int. Electron Devices Meeting Tech. Dig.*], 37.3.1 – 37.3.4, IEEE, New York (2009).

[12] Lam, K.-T., Lee, C., and Liang, G., "Bilayer graphene nanoribbon nanoelectromechanical system device: A computational study," *Applied Physics Letters* **95**(14), 143107 (2009).

[13] Banerjee, S. K., Register, L. F., Tutuc, E., Reddy, D., and MacDonald, A. H., "Bilayer pseudospin field-effect transistor (bisfet): A proposed new logic device," *IEEE Elect. Dev. Lett.* **30**(2), 158 – 160 (2009).

[14] Williams, J. R., DiCarlo, L., and Marcus, C. M., "Quantum hall effect in a gate-controlled p-n junction of graphene," *Science* **317**(5838), 638–641 (2007).

[15] Gorbachev, R. V., Mayorov, A. S., Savchenko, A. K., Horsell, D. W., and Guinea, F., "Conductance of p-n-p graphene structures with "air-bridge" top gates," *Nano Letters* **8**(7), 1995–1999 (2008). PMID: 18543979.

[16] Liu, G., Velasco, J. J., Bao, W., and Lau, C. N., "Fabrication of graphene p-n-p junctions with contactless top gates," **92**(20), 203103 (2008).

[17] Do, V. N., Nguyen, V. H., Dollfus, P., and Bournel, A., "Electronic transport and spin-polarization effects of relativisticlike particles in mesoscopic graphene structures," **104**(6), 063708 (2008).

[18] Ren, H., Li, Q.-X., Luo, Y., and Yang, J., "Graphene nanoribbon as a negative differential resistance device," *Applied Physics Letters* **94**(17), 173110 (2009).

[19] Fang, H., Wang, R.-Z., Chen, S.-Y., Yan, M., Song, X.-M., and Wang, B., "Strain-induced negative differential resistance in armchair-edge graphene nanoribbons," **98**(8), 082108 (2011).
[20] Do, V. N. and Dollfus, P., "Negative differential resistance in zigzag-edge graphene nanoribbon junctions," *Journal of Applied Physics* **107**(6), 063705 (2010).
[21] Nguyen, V. H., Bournel, A., and Dollfus, P., "Large peak-to-valley ratio of negative-differential-conductance in graphene p-n junctions," **109**(9), 093706 (2011).
[22] Habib, K. M. M., Zahid, F., and Lake, R. K., "Negative differential resistance in bilayer graphene nanoribbons," *Applied Physics Letters* **98**(19), 192112 (2011).
[23] González, J. W., Santos, H., Pacheco, M., Chico, L., and Brey, L., "Electronic transport through bilayer graphene flakes," *Phys. Rev. B* **81**(19), 195406 (2010).
[24] Tomfohr, J. and Sankey, O. F., "Theoretical analysis of electron transport through organic molecules," *J. Chem. Phys.* **120**(3), 1542 – 1554 (2004).
[25] Bruque, N. A., Pandey, R. R., and Lake, R. K., "Electron transport through a conjugated molecule with carbon nanotube leads," *Phys. Rev. B* **76**(20), 205322 (2007).
[26] J. W. González, H. Santos, E. Prada, L. Brey, and L. Chico, Gate-controlled conductance through bilayer graphene nanoribbons, arXiv:1008.3255v1[cond-mat.mes-hall] (2010).